and the monomeric friction coefficient which control the diffusion of homopolymers into homopolymer diffusion. It has also been shown that the rate of solvent evaporation and annealing treatments of the host copolymer markedly influence the structure as seen by changes in the transport properties. Finally, reorganization processes may occur at the homopolymer–copolymer interface or in the bulk. However, the time scales for this are very much different than that of the diffusion process.

Acknowledgment. We thank H. Ito of the IBM Almaden Research Center for providing the deuterated PMMA. We thank Dr. T. Christensen for the XPS measurements on the copolymer specimens. R.J. is grateful to the IBM World Trade Organization and to the IBM Almaden Research Center for the possibility of visiting the latter facility. M.G. and R.J. are very much indebted to "Services de la Programmation de la Politique Scientifique" (Brussels) for financial support. M.G. thanks the Fonds National de la Recherche Scientifique for a fellowship. Part of this work was performed at the Sandia National Laboratories and was supported by the U.S. Department of Energy under Contract DE-AC04-76DP00789.

Registry No. (S)(MMA) (copolymer), 106911-77-7.

References and Notes

(1) For a recent review see: Tirrell, M. V. *Rubber Chem. Tech.* **1984**, *57*, 523.
(2) Doi, M.; Edwards, S. F. *J. Chem. Soc., Faraday Trans. 2* **1978**, 1978, 1809, 1818.
(3) deGennes, P. G. *J. Chem. Phys.* **1971**, *55*, 572.
(4) Graessley, W. W. *J. Polym. Sci., Polym. Phys. Ed.* **1980**, *18*, 27.
(5) Hasegawa, H.; Hashimoto, T. *Macromolecules* **1985**, *18*, 589.
(6) Ouhadi, T.; Fayat, R.; Jérôme, R.; Teyssie, Ph. *Polymn. Commun.* **1986**, *27*, 212; U.S. Patent 4 461 874, 1984.
(7) Ito, H.; Russell, T. P.; Wignall, G. D. *Macromolecules*, in press.
(8) Russell, T. P.; Koberstein, J. T. *J. Polym. Sci., Polym. Phys. Ed.* **1985**, *23*, 1109.
(9) Green, P. F.; Christensen, T. M.; Russell, T. P. *Macromolecules*, in press.
(10) Mills, P. J.; Green, P. F.; Palstrom, C. J.; Mayer, J. W.; Kramer, E. J. *Appl. Phys. Lett.* **1984**, *45*, 958.
(11) Green, P. F.; Mills, P. J.; Kramer, E. J. *Polymer* **1986**, *27*, 1063.
(12) Green, P. F.; Doyle, B. L. *Nucl. Instrum. Meth. Phys. Res., Sect. B* **1986**, *B18*, 64.
(13) Benoit, H.; Wu, W.; Benmouna, M.; Mozer, B.; Bauer, B.; Lapp, A. *Macromolecules* **1985**, *18*, 986.
(14) Leibler, L. *Macromolecules* **1980**, *13*, 1602.
(15) Ohta, T.; Kawasaki, K. *Macromolecules* **1986**, *19*, 2621.
(16) Russell, T. P.; Jérôme, R., in preparation.
(17) Wu, S. *Polymer Interfaces and Adhesion*; Marcel Dekker: New York, 1982.
(18) In cases where one tries to diffuse d-PMMA into PS one obtains what appears to be a diffusion profile. This results from the fact that the PMMA forms very small spherical particles on the surface of PS, and since PS is viscous, these spherical particles become incorporated into the PS matrix. This occurs over a certain molecular weight regime, and the behavior is not consistent from one temperature to another.
(19) Whitmore, M. D.; Noolandi, J. *Macromolecules* **1985**, *18*, 2486.
(20) Green, P. F.; Russell, T. P.; Jérôme, R.; Granville, M. *Macromolecules*, in press.
(21) Graessley, W. W. *Faraday Symp. Chem. Soc.* **1983**, *No. 18*, 1.
(22) Hashimoto, T.; Nagatoshi, K.; Todo, A.; Hasegawa, H.; Kawai, H. *Macromolecules* **1974**, *7*, 364.
(23) Henkee, C. S.; Thomas, E. L.; Fetters, L. J. *J. Mater. Sci.*, in press.

Predictions of the Ability of Solution Dynamics Experiments to Characterize Long-Chain Structure in Flexible Homopolymers

Robert L. Sammler† and John L. Schrag*

Department of Chemistry and Rheology Research Center, University of Wisconsin, Madison, Wisconsin 53706. *Received December 17, 1987; Revised Manuscript Received April 8, 1988*

ABSTRACT: Extensive predictions are presented to illustrate the ability of linear viscoelasticity and oscillatory flow birefringence experiments to characterize long-chain structure in flexible homopolymers. The predicted dilute-solution, low-shear-rate dynamic properties are based on a recent generalization of the bead–spring model that enables such properties to be computed efficiently for any chain of identical beads connected by Hookean springs. Highly symmetric chains with linear, star, H, comb, ring, or cyclic-comb geometry are emphasized. Ways to identify samples with these geometries from their solution properties are presented, as well as ways to characterize the sizes of the branches and backbone, the number of branches, and location of branches attached to the backbone. Characterization is expected to be difficult only for small chains and for the determination of the number of branches in star or starlike chains when it exceeds about 8.

I. Introduction

Long-chain branches attached to straight-chain or cyclic backbones are common and distinctive structural features of macromolecules and yet their characterization, in terms of branch and backbone size or the number and location of the branches, remains challenging even for the simplest highly symmetric chains. The potential of solution dynamics measurements for characterization of such structural features was recognized long ago. However, only in the last 15 years have there been sufficient advances in both the measurement and quantitative prediction of solution dynamics to enable a pragmatic evaluation of this potential. Flow properties such as the complex viscosity coefficient η^* (linear viscoelasticity (VE) experiments[1–6]) and the complex mechanooptic coefficient S^* (linear oscillatory flow birefringence (OFB) experiments[3–8]) can now be measured over many decades of shearing frequency with sufficient accuracy to be extrapolated to infinite dilution; such data are required to probe the wide range of time scales associated with conformational motions of macromolecules in solution and to interpret long-chain structure from dynamic properties in which interchain interactions are negligible. Bead–spring models are now formulated[9,10] to enable predictions of such properties to be efficiently and accurately computed for an idealized flexible homopolymer chain of any geometry, for chains of finite size, and for any degree of hydrodynamic interaction; these computations are needed for the assessment of long-chain

†Current address: Polymer Products Department, Experimental Station, E. I. du Pont de Nemours and Co., Inc., Wilmington, DE 19898.

0024-9297/88/2221-3273$01.50/0

structural features from data measured in Θ and non-Θ solvents. In this paper selected results of these computational methods are presented to illustrate the ability of VE and OFB experiments to characterize long-chain structure in flexible homopolymers. The predictions are for regular chains with linear, star, H, comb, ring, and cyclic-comb chain geometries. High molecular weight homopolymer samples of such chains with narrow polydispersities, most applicable to these predictions, have been prepared or are synthetically feasible. A section is devoted to each chain geometry, exploring the effect on the solution dynamics of the number, size, and location of straight-chain branches attached to a straight-chain or cyclic backbone; modifications of these effects caused by variation of the degree of hydrodynamic interaction are also studied. All predicted properties for such idealized chains are computed exactly so that any discrepancy between them and those measured may be attributed to deficiencies in the model and not to computational approximation. Experimental verification of many predictions reported here for star and comb geometries is contained in the third paper[20] of this series; it reports quantitative comparisons of theoretical predictions and experimental infinite-dilution OFB properties. As reported here and in earlier work summarized in the next section, properties computed exactly are found to fit measured properties quite well.

II. The Bead–Spring Model

Except for stars with more than eight arms, predictions of the frequency dependence of η^* or S^* for isolated chains with linear, regular star, or regular comb geometry, based on the bead-spring model (BSM), compare[2-6,8,11-19] excellently with experimental measurements (extrapolated to infinite dilution) after the solvating medium contributions are properly accounted for. The predictions are best for samples of amorphous homopolymers with narrow polydispersities which contain flexible chains with uniform tacticity and simple geometry. Good solvent conditions are also preferable based on experimental observations of solvating environment effects.[20,42-44] From these comparisons we expect BSM predictions will similarly describe the properties of homopolymers having more complicated long-chain structure as long as the extent of branching at each branch site remains moderate (<10).

The bead–spring model used here represents a flexible homopolymer as a chain of identical spherical beads connected by identical springs. It incorporates springs with a Hookean force law, the "preaveraging" treatment of hydrodynamic interaction, and Gaussian statistics. Interchain interactions and sample polydispersity are not considered. Although there are several important versions and formulations of this model,[9,21-28] all predictions shown here are from a recent formulation[10] applicable to any assortment of beads and springs that enables computation of properties of such idealized chains with the exact eigenvalue algorithm used by Lodge and Wu.[9] The efficiencies gained from use of a formulation applicable to this algorithm have facilitated the computation of the properties of large macromolecules; properties of chains containing up to 3000 springs—typically corresponding to about 10^7 in molecular weight—can be easily computed. Moreover, it is also possible to compute the exact properties of still larger chains for linear, regular star, regular H, or ring geometries since new block-diagonal forms of **L** have been obtained.[10]

A. Small-Amplitude Oscillatory Flow Properties. The spatially invariant rate of shear $\dot{\gamma}$ in small-amplitude oscillatory flow experiments (narrow gap limit)[29] varies sinusoidally in time with angular frequency ω and amplitude $\dot{\gamma}^0$. The complex mechanooptic coefficient S^*, the complex viscosity coefficient η^*, and the dynamic shear modulus G^* of such flow experiments are predicted to be

$$S^* = q'nb^2\sum_p \frac{\tau_p}{1 + i\omega\tau_p} + S_e \quad (1)$$

$$\eta^* = nkT\sum_p \frac{\tau_p}{1 + i\omega\tau_p} + \eta_e \quad (2)$$

$$G^* = nkT\sum_p \frac{i\omega\tau_p}{1 + i\omega\tau_p} + i\omega\eta_e \quad (3)$$

with q' an optical factor, n the number density of chains in solution, b^2 the mean-square distance between connected beads in a nonflowing solution, k the Boltzmann constant, T the absolute temperature, τ_p the relaxation time for the pth mode, $i = (-1)^{1/2}$, and $\sum_p$ indicating a sum over all N normal modes. S_e and η_e are frequency-independent terms usually dominated by chain environment contributions; historically they have been assumed to be identical with bulk solvent properties (S_s and η_s) or ϕS_s and $\phi\eta_s$ where ϕ is the volume fraction of solvent, although recent experimental work shows these to be incorrect, in general. For the special case of an isorefractive homopolymer/solvent system, the optical factor is related to the index of refraction n_s of the solvent and the intrinsic optical anisotropy $(\alpha_1 - \alpha_2)$ of the Kuhn statistical segment by

$$q' = \frac{4\pi}{45}\frac{(n_s^2 + 2)^2}{n_s}\frac{\alpha_1 - \alpha_2}{b^2} \quad (4)$$

In general, each relaxation time τ_p is inversely proportional to λ_p, one of the N positive and possibly degenerate eigenvalues of the real symmetric matrix **L**.[10]

$$\tau_p = \frac{b^2\zeta}{6kT\lambda_p} \quad (5)$$

Here ζ is the bead friction coefficient. The relaxation times are customarily assembled in decreasing order ($\tau_1 \geq \tau_2 \geq \ldots \tau_N$). As demonstrated in section IV, the spacings of the relaxation times (or λ_p) can be dramatically affected by chain size and chain geometry, and to a lesser extent by the degree of hydrodynamic interaction; the number of relaxation times is only affected by chain size. The ways to accurately compute all of the λ_p are limited; the problem becomes acute as the complexity of the chain increases, especially when intermediate degrees of hydrodynamic interaction are involved. These computations are the subject of section III.

B. Intrinsic Properties and Their Reduced Formats. The portion of the solution dynamics intrinsic to idealized isolated chains is obtained via the following extrapolations to infinite dilution: $[S^*]_\Delta = \lim_{c\to 0}(S^* - S_e)/c$, $[\eta^*]_\Delta = \lim_{c\to 0}(\eta^* - \eta_e)/\eta_e c$, and $[G^*]_\Delta = \lim_{c\to 0}(M/cRT)(G^* - i\omega\eta_e)$. $[S^*]_\Delta$, $[\eta^*]_\Delta$, and $[G^*]_\Delta$ are coefficients called the modified intrinsic birefringence, modified intrinsic complex viscoelasticity, and modified intrinsic reduced dynamic shear modulus, respectively; R is the ideal gas constant, N_a is Avagadro's number, M is the molecular weight of the idealized chain, and c is the polymer concentration in grams per milliliter. BSM predictions are most applicable to these infinite dilution properties. Experimentally, S_e and η_e have recently been approximated by S'_∞ or η'_∞—frequency-independent solution properties observed at high frequency. These quantities appear to be the proper frequency-independent quantities to isolate the chain dynamics contribution for most solutions, although this is the subject of current study.[6,30,31]

Expressing these coefficients in phasor format is of particular interest since the angles $[\Theta_\Delta]$ and $[\Phi_\Delta]$, obtained from $[S^*]_\Delta = [S_{M\Delta}] \exp\{+i[\Theta_\Delta]\}$ and $[\eta^*]_\Delta = [\eta_{M\Delta}] \exp\{-i[\Phi_\Delta]\}$, are very sensitive to the effects of long-chain structure. From eq 1 and 2 the magnitude $[S_{M\Delta}]$ and angle $[\Theta_\Delta]$ of the intrinsic birefringence are predicted to be

$$[S_{M\nabla}] = \frac{|q'|b^2N_a}{M}\left[\left(\sum_p \frac{\tau_p}{1+\omega^2\tau_p^2}\right)^2 + \left(\sum_p \frac{\omega\tau_p^2}{1+\omega^2\tau_p^2}\right)^2\right]^{1/2} \quad (6)$$

$$[\Theta_\Delta] = -\tan^{-1}\left(\frac{\sum_p \frac{\omega\tau_p^2}{1+\omega^2\tau_p^2}}{\sum_p \frac{\tau_p}{1+\omega^2\tau_p^2}}\right) \pm \left(1 - \frac{q'}{|q'|}\right)\frac{\pi}{2} \quad (7)$$

and the magnitude $[\eta_{M\Delta}]$ and angle $[\Phi_\Delta]$ of the intrinsic complex viscoelasticity to be

$$[\eta_{M\Delta}] = \frac{RT}{M\eta_s}\left[\left(\sum_p \frac{\tau_p}{1+\omega^2\tau_p^2}\right)^2 + \left(\sum_p \frac{\omega\tau_p^2}{1+\omega^2\tau_p^2}\right)^2\right]^{1/2} \quad (8)$$

$$[\Phi_\Delta] = +\tan^{-1}\left(\frac{\sum_p \frac{\omega\tau_p^2}{1+\omega^2\tau_p^2}}{\sum_p \frac{\tau_p}{1+\omega^2\tau_p^2}}\right) \quad (9)$$

The similarity of both sets of expressions indicates the complementary nature of OFB and VE properties expected for flexible homopolymers; the frequency dependence of the magnitudes should be the same (neglecting proportionality constants) and the angles should be linearly related at each frequency by

$$[\Theta_\Delta] = -[\Phi_\Delta] \pm (1 - q'/|q'|)\pi/2 \quad (10)$$

(Differences in the sign of q' for several polymers investigated to date have been particularly helpful in separating contributions of the chain from those of the solvent.[6]) The predicted similarities in OFB and VE properties are even more pronounced when they are expressed in a reduced format obtained by dividing each coefficient by its low-frequency limiting value.

$$[S_0]_\Delta = \lim_{\omega\to 0}[S^*]_\Delta = [S_{M\Delta 0}] \exp\{+i[\Theta_{\Delta 0}]\} \quad (11)$$

$$[\eta_0]_\Delta = \lim_{\omega\to 0}[\eta^*]_\Delta = [\eta_{M\Delta 0}] \exp\{-i[\Phi_{\Delta 0}]\} \quad (12)$$

The resulting expressions for the reduced magnitudes and angles are

$$\frac{[\eta_{M\Delta}]}{[\eta_{M\Delta 0}]} = \frac{[S_{M\Delta}]}{[S_{M\Delta 0}]} = \left[\left(\sum_p \frac{\lambda_1/\lambda_p}{1+(\omega\tau_1)^2(\lambda_1/\lambda_p)^2}\right)^2 + \left(\omega\tau_1\sum_p \frac{(\lambda_1/\lambda_p)^2}{1+(\omega\tau_1)^2(\lambda_1/\lambda_p)^2}\right)^2\right]^{1/2} / \sum_p(\lambda_1/\lambda_p) \quad (13)$$

and

$$[\Phi_\Delta] - [\Phi_{\Delta 0}] = -([\Theta_\Delta] - [\Theta_{\Delta 0}]) = + \tan^{-1}\left(\frac{\omega\tau_1\sum_p \frac{(\lambda_1/\lambda_p)^2}{1+(\omega\tau_1)^2(\lambda_1/\lambda_p)^2}}{\sum_p \frac{\lambda_1/\lambda_p}{1+(\omega\tau_1)^2(\lambda_1/\lambda_p)^2}}\right) \quad (14)$$

When defined in this way, the reduced angle for both the OFB and VE properties varies between 0 and +90°. The advantages of using these reduced formats are 2-fold. First, the effects of (bead–spring) chain structure and hydrodynamic interaction are highlighted, since the reduced formats are only functions of the set of N eigenvalues. Second, since predictions for the reduced OFB and VE properties are identical, either OFB notation (employed here) or VE notation may be used interchangeably. (Note that although both experiments are predicted to provide identical long-chain characterization information, OFB data frequently have been more useful because the environmental contribution (S_e) for birefringence data is usually a much smaller fraction of the measured properties than is the corresponding quantity (η_e) for viscoelasticity.[6] Currently, OFB instrumentation is not commercially available; VE instrumentation is available but it is not designed to provide dilute-solution properties with the precision or accessible frequency range required for characterizations of the long-chain structure of interest here. The precision of VE instrumentation and the associated computerized data acquisition systems in this laboratory have recently been upgraded; the resultant measurement precision (ca. 0.1% deviation) is such that VE and OFB characterization capabilities are now comparable.[1-6,31])

C. Parameters Representing Long-Chain Structure and Hydrodynamic Interaction. The intrinsic properties in reduced format are a function of the N eigenvalues of the **L** matrix and therefore only depend on the (bead–spring) chain structure and the degree of preaveraged hydrodynamic interaction. The structure of chains with linear, regular star, regular H, regular comb, ring, and regular cyclic-comb geometries is represented with one or more of a set of three dimensionless parameters. The set of chain structure parameters used here—f, n_b, and n_0—best describe chains composed of straight-chain branches of equal size attached at regular intervals to a straight-chain or cyclic backbone. The number of branches attached to the backbone is f, while n_b is the number of beads in each of the branches (excludes the bead at the branch site), and n_0 is the number of backbone beads between adjacent branches (excludes the beads at the branch sites). The functionality of branch sites is 3 for the two sites in H chains, 3 for the f branch sites in combs and cyclic combs, and equal to the number of branches (f) for the single site in stars. Chains with linear and ring geometries are simply represented with n_0; chains with regular star geometry are represented with f and n_b; and chains with regular H geometry are represented with n_b and n_0. Combs and cyclic combs use all three parameters. A summary of the chain structure parameters for six simple chain geometries and of the total number of beads N_b, springs N_s, normal modes N, and springs in the longest contiguous span N_{span} is found in Table I. The use of such parameters is illustrated in Table II. All represent long-chain structural features of homopolymers which are potentially deducible from fits of theoretical predictions to measured dilute-solution dynamic properties.

The degree of hydrodynamic interaction is specified by the dimensionless parameter h^* of Thurston and Peterlin.[32] It is used here regardless of the bead–spring chain structure.

$$h^* = \frac{\zeta}{\eta_e}\left(\frac{1}{12\pi^3b^2}\right)^{1/2} \quad (15)$$

It is preferred over the h originally used by Zimm[23] because it is expected to be independent of chain size. The so-

Table I
Summary of Chain Structure Parameters

chain geometry	chain params	N_b	N_s	N	N_{span}
linear	n_0	n_0	$n_0 - 1$	$n_0 - 1$	$n_0 - 1$
ring	n_0	n_0	n_0	$n_0 - 1$	
regular star	f, n_b	$fn_b + 1$	fn_b	fn_b	$2n_b$
regular H	n_b, n_0	$2 + n_0 + 4n_b$	$1 + n_0 + 4n_b$	$1 + n_0 + 4n_b$	$1 + n_0 + 2n_b$
regular cyclic comb	f, n_b, n_0	$f(n_0 + n_b + 1)$	$f(n_0 + n_b + 1)$	$f(n_0 + n_b + 1) - 1$	
regular comb	f, n_b, n_0	$f(n_0 + n_b + 1) + n_0$	$f(n_0 + n_b + 1) + n_0 - 1$	$f(n_0 + n_b + 1) + n_0 - 1$	$\begin{bmatrix} f(n_0 + 1) + n_0 - 1, & n_0 \geq n_b \\ (f-1)(n_0 + 1) + 2n_b, & n_0 \leq n_b \end{bmatrix}$

called "free-draining" and "non-free-draining" limits of h^* are approximately 0.00 and 0.25, respectively. (The $h^* = 0.00$ limit is not physically realistic since it implies there is no viscous dissipation of energy ($\zeta = 0$) by the chain. Thus whenever h^* is shown equal to zero, it implies the limit $h^* \to 0$.) The non-free-draining limit was estimated by Osaki[33] for linear chains and, as it turns out, this estimate is very good for any chain composed of identical beads connected by identical Hookean springs.

III. Computation of Eigenvalues

The eigenvalues of **L** are computed numerically with a general algorithm applicable to any real, symmetric, and possibly singular matrix. Eigenvalues are computed directly from **L** and/or from more concise, block-diagonal forms for linear, regular star, regular H, or ring chains. The eigenvalue algorithm and estimates of eigenvalue accuracy are described below. The algorithm is basically that used by Lodge and Wu[9] for linear chains; it has been altered for use on a Harris/7 or VAX 8600 computer and to decrease its virtual memory requirements so that properties of very large chains can be computed.

A. The QR Algorithm. The first step in the algorithm is the transformation of the symmetric matrix of order N_s into tridiagonal form. It is accomplished with $N_s - 2$ similarity transformations by using Householder matrices.[34] The algorithm takes advantage of the symmetry of both **L** and the Householder matrices. Only the lower triangular portion of **L** is stored and matrices are multiplied without ever storing more than a single row of elements for each Householder matrix. Even with these efficiencies the tridiagonalization requires much more memory and many more computations than the subsequent iterative portion of the eigenvalue algorithm. The second step in the algorithm is the transformation from tridiagonal to diagonal form with the QR method and shifts of origin.[34] Each shift accelerates the convergence of the lower right off-diagonal element to zero. After several iterations, the lower right off-diagonal element becomes less than a specified minimum residual; the lower right diagonal element is then saved as an eigenvalue and the order of the matrix is reduced by one. This process is repeated $N_s - 1$ times, and the N_s eigenvalues are then sorted into increasing order. For chains with N_c cyclic structures, the first N_c eigenvalues are essentially zero and indicate the number of times the set of N_s connector coordinates are linearly dependent. These N_c eigenvalues are discarded and the remaining eigenvalues renumbered. We have observed that all eigenvalues computed in this manner for Gaussian bead–spring chains are positive or zero regardless of chain geometry for h^* between 0.00 and 0.25. Negative eigenvalues can appear when h^* approaches or exceeds 0.30.

B. Reliability and Accuracy. The reliability of the FORTRAN software[5] used to generate **L** and compute its eigenvalues was checked in several direct and indirect ways. The direct ways all employed the limited number of closed-form eigenvalue expressions currently available only for rings;[35] chains with linear, regular star, or regular H geometries under free-draining hydrodynamic interaction conditions; or chains composed of up to about eight springs. Other checks of software reliability include verifying that (1) the eigenvalues of **L** and its more concise block-diagonal forms for linear, regular star, regular H, and ring chains are the same; (2) the eigenvalues of a chain are independent of the numbering of the beads and springs (e.g., an f-armed regular star with n_b beads per arm has the same eigenvalues when represented as a structure composed of a single backbone bead with f arms attached to it or as a structure composed of $2n_b + 1$ backbone beads with $f - 2$ arms attached to the center backbone bead); (3) the eigenvalues of very large linear, regular star, or ring chains in the non-free-draining limit agree with well-known results based on integrodifferential equations; and (4) the

Table II
Examples of Usage of Bead–Spring Chain Structure Parameters

molecular geometry	f	n_b	n_0	chain structure[a]
linear	0		4	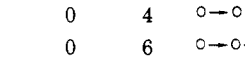
	0		6	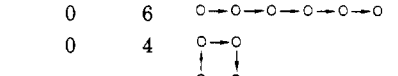
ring	0		4	
	0		6	
regular star	3	2		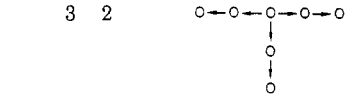
	4	1		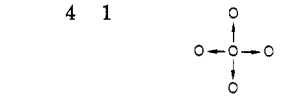
regular comb	3	2	0	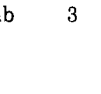
	2	3	1	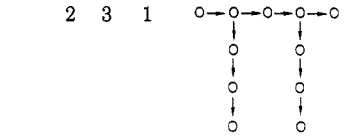
regular H	4	1	0	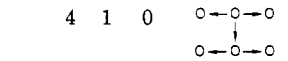
	4	3	1	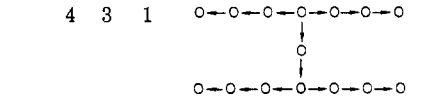
regular cyclic comb	3	2	0	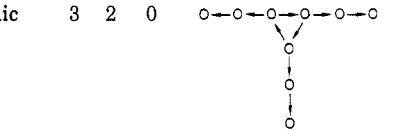
	2	3	1	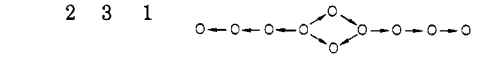

[a] 0 and → represent a bead and a connector vector, respectively.

eigenvalues (and functions of eigenvalues) for linear, regular star, and comb geometry agree with those reported[9,26,27,36-38] previously.

Eigenvalue accuracy was investigated with closed-form eigenvalue expressions and with computations at the various levels of numerical precision available to the particular computer in use. Any error found is attributable to round-off error since all mathematical operations employed are exact. Regardless of chain size, geometry, or degree of hydrodynamic interaction the accuracy of the eigenvalues on the Harris/7 is $\pm 10^{-7}$ (or $\pm 10^{-15}$) when real numbers are represented in double (or quadruple) precision with 34 (or 70) bit mantissas and 8 (or 24) bit exponents. For the majority of the eigenvalues ($1 < \lambda_p < 10$) this translates into 8 (or 16) significant figures. However, the relative accuracy of the smaller eigenvalues ($0 < \lambda_p < 1$) decreases as $\lambda_p \to 0$. These smaller eigenvalues are very important because they dominate the low-frequency dynamic properties and contain most of the chain geometry characterization information. To estimate the number of significant figures for these eigenvalues the worst case was chosen—the smallest eigenvalue of a free-draining linear chain. The closed form expression for this eigenvalue is

$$\lambda_1 = 4 \sin^2 \left(\frac{\pi}{2(N_s + 1)} \right) \tag{16}$$

and no chain has a smaller eigenvalue if it is composed of N_s springs or less, or if its longest contiguous span is less than N_s springs. Using the absolute accuracies provided above, this eigenvalue would be accurate to three significant figures at an N_s of 993 (or 9.9×10^7) if it was computed in double (or quadruple) precision. Thus for smaller chains all eigenvalues would be correct to three or more significant figures. These concepts were used to ensure all properties reported were based on eigenvalues accurate to at least three significant figures. Copies of the software—or the eigenvalue spectra used to generate the reduced dynamic properties reported here—are available on request. This software is applicable to any comb or cyclic comb and not just to the six chain geometries reported here; we have found this feature useful for investigating the properties of irregular chains, which are invariably present to some degree as polydispersity components in real samples.

IV. Predictions of the Effects of Long-Chain Structure

The effects of long-chain structure and hydrodynamic interaction on the frequency dependence of $[S^*]_\Delta/[S_0]_\Delta$ are computed with eq 13 and 14. The chain structural features of most interest are the sizes of straight-chain or cyclic backbones, the number and size of straight-chain branches attached to the backbone, and the size of the (regular) interval between the branches. The logarithm of the reduced magnitude log $([S_{M\Delta}]/S_{M\Delta 0}])$ and the reduced angle $-([\Theta_\Delta] - [\Theta_{\Delta 0}])$ are both plotted as ordinates against the logarithm of the reduced angular shearing frequency log $(\omega\tau_1)$. The frequency dependence of the angle is much more sensitive to the effects under study and therefore is highlighted in all of the remaining sections.

In each plot the reduced frequency ranges from 10^{-2} to 10^7. Intrinsic to this range are three frequency regimes that are separated by two transition zones near $\omega\tau_1 = 1$ and $\omega\tau_1 = \tau_1/\tau_N$. The regime between these transition zones is most important for the investigation of long-chain structure. Qualitatively, the magnitude of $[S^*]_\Delta/[S_0]_\Delta$ decreases monotonically from unity to zero with increasing frequency. The slope of the descent is smallest at low frequency, becomes markedly steeper in each transition zone, and reaches a maximum at high frequency where the magnitude becomes inversely proportional to frequency. Concomitantly, the reduced angle gently rises from 0° at low frequency, climbs steeply in the first transition zone, levels to a "plateau" region, climbs steeply again in the second transition zone, and finally approaches its maximum of 90° at high frequency. The "plateau" region may contain one or two sublevels (subplateaus) or have one local minimum and maximum at the lower frequencies. For the chain geometries investigated here, most often the angle changes monotonically with frequency; the local extrema are only found for highly branched ($f > 4$) stars, starlike ($n_0/n_b \ll 1$) combs, or cyclic combs when they have a wide gap in their relaxation time spectrum. Generally, the steepness of the angle curve in the low-frequency transition zone and the number of subplateaus and/or local extrema in the plateau region are predicted to be important features for identification of chain geometry. The width of the whole plateau characterizes the size of the longest contiguous span within the chain; the width of the higher level high-frequency subplateau, when present, characterizes the intrachain length $2n_b$, $2n_b + n_0 + 1$, or $2n_b + (n_0 + 1)(1 - f^{-1})$ (equivalent) springs depending on the chain geometry. The level of the plateau indicates the degree of hydrodynamic interaction and/or the functionality of the branch sites along the backbone. Increasing the degree of hydrodynamic interaction drops the level of the whole plateau; increasing functionality of the branch sites lowers the low-frequency plateau and gently raises the high-frequency plateau when both or one is present.

To identify the transition zones and to help interpret predicted long-chain structural effects, a line spectrum of the set of discrete relaxation times is also shown on the plots. Each of the N vertical lines in the set represents a normal mode of motion of the bead–spring chain. The lines are drawn at points along the reduced frequency axis where $\omega = 1/\tau_p$ so that

$$\omega\tau_1 = \tau_1/\tau_p = \lambda_p/\lambda_1 \tag{17}$$

for mode p ($p = 1, 2, 3, \ldots, N$). The spacing between adjacent relaxation times usually decreases with increasing mode number. The longer relaxation times are well separated while the shorter are so closely spaced that they appear like a continuum on the plots. When degeneracies occur, the individual lines are drawn such that the height of the line is proportional to the degeneracy.

The properties of several chains are always displayed on a single plot; a convention has been introduced to avoid explicit labeling of each relaxation time spectrum and each curve of reduced magnitude or angle. The model parameters under study are listed to the left of each relaxation time spectrum; those parameters held fixed are shown in the box on the right side of the figure. The labeling for both the magnitude and angle curves is implied from the sequence in which the relaxation time spectra are drawn. It takes advantage of our usual choice to order the spectra such that their breadth increases the lower they are drawn. The sequence corresponds to the order of descending intersection if a vertical line were drawn at $\omega\tau_1 = 10^5$; the first intersected angle (or magnitude) curve corresponds to the highest (or lowest) spectrum. The curves corresponding to the top spectrum are also distinct in that they are drawn with broken lines. The chain geometry is indicated with upper-case letters—L, S, H, C, R, CC—under the column heading CG. Use of a reduced frequency axis to display the properties of several chains on a single plot artificially aligns the τ_1 regime of each chain. Use of an absolute frequency axis (not shown) for the same set of

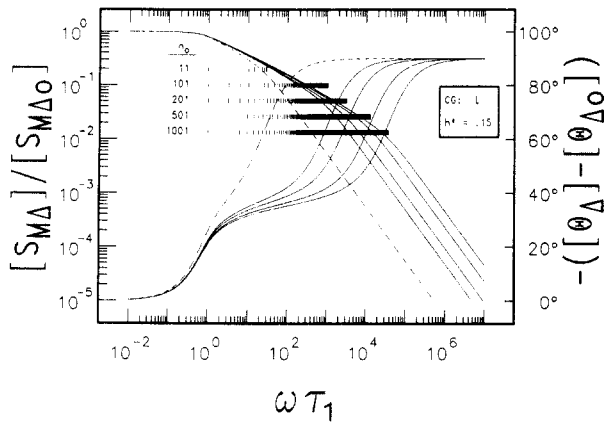

Figure 1. Effect of n_0 on predicted properties for linear chains. Curves corresponding to the top spectrum are drawn with broken lines. The other curves are identified with the order of intersection of a descending vertical line drawn at $\omega\tau_1 = 10^5$ and the height at which the spectra are drawn; the first intersected angle (or magnitude) curve corresponds to the highest (or lowest) spectrum.

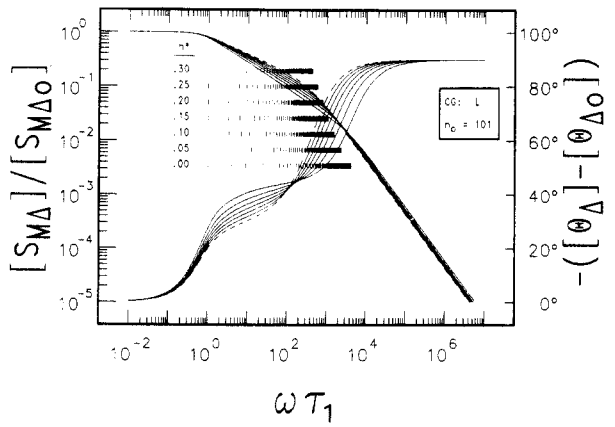

Figure 2. Effect of h^* on predicted properties for linear chains.

chains, and preferably for the same degree of hydrodynamic interaction, would roughly align the shortest relaxation time of each chain; the shortest relaxation time depends primarily on the degree of hydrodynamic interaction rather than chain size or chain geometry. Predicted properties in this alternate format closely approximate the superposition of dynamic data measured for homopolymers dissolved in the same solvent.

A. Linear Chains. The frequency dependence of $[S^*]_\Delta/[S_0]_\Delta$ for several linear chains is illustrated in Figures 1 and 2. These figures, as well as the next figures for regular stars, serve as references for later comparisons with predictions for the other chain geometries. Characteristic of linear chains[23,39,40] are nondegenerate relaxation times, a longest relaxation time that is substantially larger than the others, and a single-level plateau region in the reduced angle. The reduced properties are functions of n_0 and h^* where n_0 is proportional to the contour length of the backbone (the longest continguous span in the chain). The effects due to varying n_0 are shown in Figure 1 at an intermediate degree of hydrodynamic interaction. Increasing n_0 increases the number of relaxation times and the spectral breadth, which causes the breadth of the plateau region to lengthen. The effects of h^* are shown in Figure 2 for chains with the same n_0. Increasing h^* redistributes the spacings of the $n_0 - 1$ relaxation times and compresses their overall breadth, lowering the level and reducing the breadth of the plateau region of the angle curves. The level of the low-frequency portion of the reduced-angle plateau for large chains ($n_0 > 100$) is of interest because it depends only on h^*; at $\omega\tau_1 = 10$, it starts at about 41° and drops to 31° as h^* increases from 0 to 0.30.

For linear chains of at least 100 beads, the spacings of the longer relaxation times are weakly dependent on n_0. This dependence is illustrated in Figure 1. The spacings depend only on h^* for infinitely long chains; they have been reported by Rouse[22] and Zimm[23] at the free-draining and non-free-draining limits, respectively. For the first six modes the τ_1/τ_p ratios are

$$1, 4, 9, 16, 25, 36, \ldots \quad \text{for} \quad h^* = 0.00$$

and

$$1, 3.17, 5.99, 9.38, 13.2, 17.5, \ldots \quad \text{for} \quad h^* = 0.25$$

These results agree with our exact eigenvalue computations to two or more significant figures when n_0 exceeds 100. They also indicate that τ_1 is larger than the other τ_p in long linear chains by a factor of 3 or more.

The breadth of the relaxation time spectrum and/or the breadth of the plateau region can be characterized by the ratio $\tau_1/\tau_N = \lambda_N/\lambda_1$. This ratio is estimated for long chains at the two limiting degrees of hydrodynamic interaction by using expressions for infinitely long chains and noting from our computations at finite N that the largest eigenvalue λ_N is about 2.29 for $N > 100$ and $h^* = 0.25$:

$$\begin{aligned} \tau_1/\tau_N &\simeq (2/\pi)^2 n_0^2 \quad \text{for} \quad h^* = 0.00; \quad n_0 > 100 \\ &\simeq 0.567 n_0^{1.5} \quad \text{for} \quad h^* = 0.25; \quad n_0 > 100 \end{aligned} \tag{18}$$

The exponent drops from 2 to 1.5 and the prefactor rises from 0.405 to 0.567 as h^* increases from 0.00 to 0.25. Both limiting power-law relationships indicate that the breadth has a much stronger dependence on n_0 than on h^*.

This set of predictions suggests a method of assigning model parameters n_0 and h^* when fitting predictions to dynamic properties of very dilute solutions of monodisperse samples of linear homopolymers. It is a method first recognized[39,40] and applied when only dilute-solution OFB properties were available to be fit by BSM predictions. The method works best when dynamic data measured in the same solvent are available for several samples representing a wide range of molecular weights. First, h^* is ascertained from the level of the low-frequency portion of the plateau region of the reduced angle curves unique to the high molecular weight samples of this polymer/solvent system. Second, n_0 is varied while using the established h^* until the breadth of the plateau is fit. Finally, it is verified that the frequency dependence of the reduced magnitude is also well fit for all molecular weights to ensure self-consistency. Small levels of polydispersity within the sample will not interfere with the determination of h^* since the plateau level is independent of chain size. However, polydispersity will affect the features of the low-frequency transition zone, making the assignment of (an average) n_0 difficult. This occurs even for $\bar{M}_w/\bar{M}_n$ levels as low as 1.3. Data showing that h^* has at most a weak dependence on chain size were first reported by Thurston and Schrag[39,40] with OFB properties. Since then, with the availability of high-precision infinite-dilution properties,[17] more accurate methods of obtaining BSM properties,[9,10,36] and consideration of sample polydispersity,[5] the lack of dependence of h^* on chain size is well established for linear chains of polystyrene dissolved in good solvents.

B. Regular Stars. The properties predicted for regular stars are shown in Figures 3–5. Each relaxation spectrum[24,26] is composed of a set of n_b relaxation times that are $(f-1)$-fold degenerate and a set of n_b nondegenerate relaxation times. The longest relaxation time is degenerate and much larger than all others. The shortest is nonde-

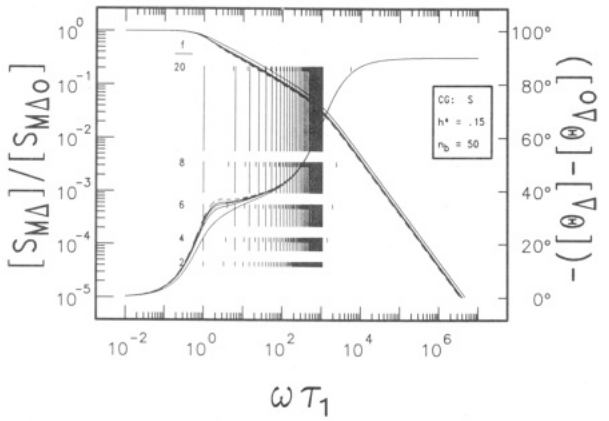

Figure 3. Effect of f on predicted properties for regular stars. Curves corresponding to the top spectrum are drawn with broken lines. The other curves are identified with the order of intersection of a descending vertical line drawn at $\omega\tau_1 = 10^0$ and the height at which the spectra are drawn.

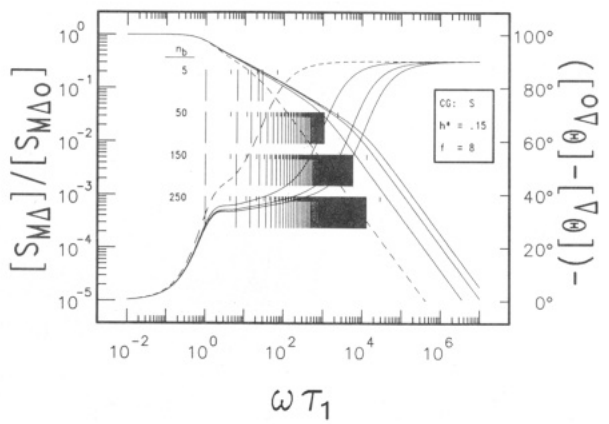

Figure 4. Effect of n_b on predicted properties for regular stars. Curves corresponding to the top spectrum are drawn with broken lines. The other curves are identified with the order of intersection of a descending vertical line drawn at $\omega\tau_1 = 10^5$.

generate and is distinctively smaller than the rest whenever $f > 2$. The rest alternate such that each nondegenerate mode falls between adjacent degenerate modes. The plateau region of the reduced angle is also unique for regular stars. Usually this region has just a single level which is equal to or higher than that observed for linear chains of similar size ($n_0 = 2n_b + 1$) and degree of hydrodynamic interaction. Sometimes there is a small local minimum and maximum in the low-frequency portion of plateau region. These extrema are always separated in frequency by at least a half decade and the maximum always occurs at a lower frequency. More generally, these extrema are characteristic of starlike chains with at least five arms attached very close to or at the same point.

The reduced properties of regular stars depend on f, n_b, and h^*. The effects of f, the number of straight-chain branches attached to a central bead, on the dynamic properties are illustrated in Figure 3 for a set of chains with $n_b = 50$ and $h^* = 0.15$. The usual convention for the identification of the reduced angle curves is of little use here since the properties are indistinguishable at $\omega\tau_1 = 10^5$; moving downward on a vertical line at $\omega\tau_1 = 1$, the order of intersection now corresponds to f of 20, 8, 6, 4, and 2. The least-branched star ($f = 2$) is a linear chain ($n_0 = 2n_b + 1$). The effect on the relaxation time spectrum of increasing f is 2-fold: it increases the degeneracy of the degenerate relaxation times (without affecting their spacings) and it increases the spacings of the nondegenerate relaxation times relative to τ_1. The latter effect is

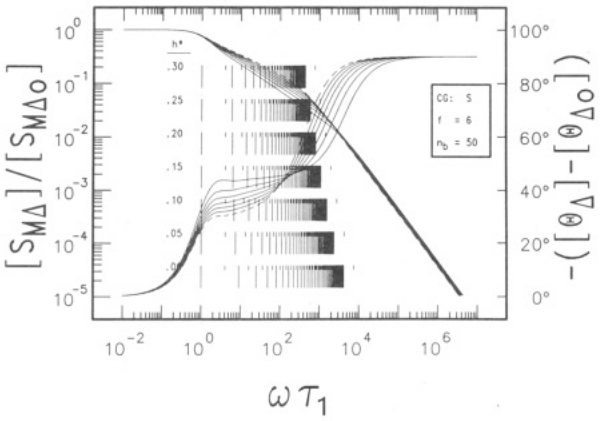

Figure 5. Effect of h^* on predicted properties for regular stars.

small for all but the shortest relaxation time which is not bounded by the adjacent set of degenerate relaxation times and is roughly inversely proportional to the functionality, f, of the single branch site. Both effects combine to raise the level of the plateau region of the reduced angle with increasing f. This level is used to characterize the value of f from measured dynamic properties. Its effectiveness for such characterizations is diminished for the more highly branched chains because $[S^*]_\Delta/[S_0]_\Delta$ depends weakly on f at large f ($f > 10$). This is an example of a more general BSM prediction—the functionality of each branch site within a chain is difficult to characterize via solution dynamic properties in the "high-frequency" plateau region when it exceeds 8. The single-level plateau of regular stars is loosely called the "high-frequency" plateau because as regular H, comb, or cyclic-comb chains become more starlike ($n_0/n_b \to 0$) their low-frequency subplateaus vanish (see Figures 6, 9, or 15) leaving only their high-frequency subplateaus.

The effects of n_b, the number of beads in each of the f straight-chain branches (proportional to the branch contour length), are shown in Figure 4 for eight-arm stars at an intermediate degree of hydrodynamic interaction. Increasing n_b increases the number and breadth of the relaxation times and spectrum, respectively, which also extends the breadth of the plateau region. For chains with long branches ($n_b \geq 50$) the spacings of the longer relaxation times are almost identical and, as a result, the level of the low-frequency portion of the plateau depends weakly on n_b.

The effects of the hydrodynamic interaction parameter h^* are illustrated in Figure 5 for a six-arm star ($f = 6$, $n_b = 50$). Larger h^* redistributes and compresses the breadth of the relaxation times; concomitantly the level of the plateau region of the reduced angle is lowered and its breadth is compressed. The level of the low-frequency portion of the plateau is independent of n_b for chains with long branches ($n_b \geq 50$). For six-arm stars it drops from about 44° to 32° at $\omega\tau_1 = 10$ as h^* increases from 0.00 to 0.30.

The breadth of the relaxation time spectrum of stars, ignoring its weakly contributing shortest relaxation time τ_N, is independent of f and can be computed from the expressions established for linear chains (eq 18, $n_0 \simeq 2n_b$):

$$\begin{aligned} \tau_1/\tau_N &\simeq (4/\pi)^2 n_b^2 \quad \text{for} \quad h^* = 0.00; \quad n_b > 50 \\ &\simeq 1.60 n_b^{1.5} \quad \text{for} \quad h^* = 0.25; \quad n_b > 50 \end{aligned} \tag{19}$$

As h^* increases from 0.00 to 0.25 the exponent drops from 2 to 1.5, but the prefactor remains virtually the same ($(4/\pi)^2 = 1.62$). The spectral breadth has a much stronger dependence on n_b (branch length) than on h^*. Similarly,

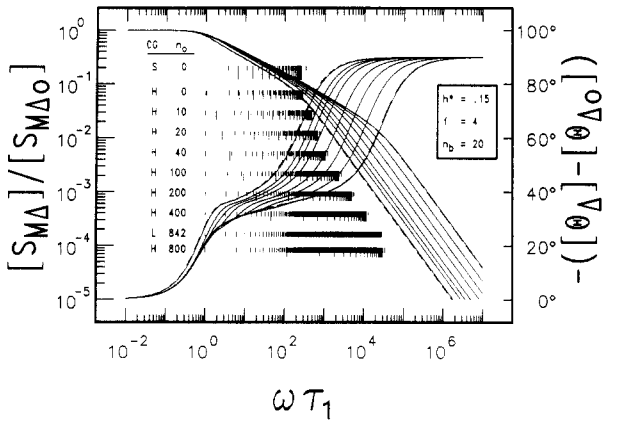

Figure 6. Effect of n_0 on predicted properties of regular H chains. Curves corresponding to the top spectrum (a regular star) are drawn with short broken lines. Curves corresponding to the linear chain are drawn with long broken lines.

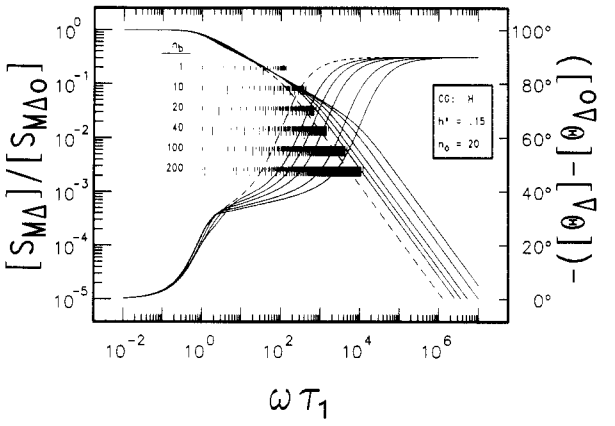

Figure 7. Effect of n_b on predicted properties for regular H chains.

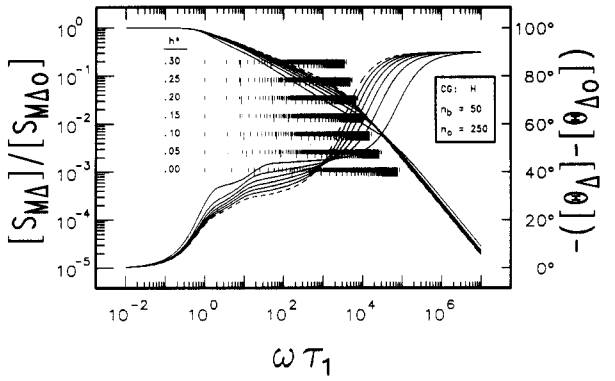

Figure 8. Effect of h^* on predicted properties for regular H chains.

the spacings of the longest degenerate relaxation times of regular stars are the same as those for the odd-indexed, longest relaxation times of linear chains. Thus the longest relaxation time of stars is approximately six times larger than any other degenerate relaxation time. For highly branched stars the nondegenerate modes contribute little to $[S^*]_\Delta/[S_0]_\Delta$, and the wide spacing between the two longest degenerate modes is responsible for the characteristic extrema observed in the low-frequency portion of the plateau region. The extrema are most distinct when f and n_b are large and h^* is small.

These predictions suggest a way to assign model parameters, f and n_b, to fit measured properties of monodisperse samples of regular stars. The method requires a preliminary experiment, as described in section IV.A, to establish h^* for the polymer/solvent system with linear chains, together with the assumption that h^* is essentially independent of f. Once h^* is established, f is varied as needed to match the level of the low-frequency portion of the (reduced-angle) plateau region to fit the measured properties. Then, n_b is adjusted to fit the breadth of the plateau. The same combination of f, n_b, and h^* will result in a quantitative description of the frequency dependence of the reduced magnitude if the parameters are correct; this should be verified. Usually a small polydispersity in the number of branches will not affect the assignment of f, or n_b, when (the average) f is large since $[S^*]_\Delta/[S_0]_\Delta$ has a weak dependence on f. Assigning n_b when there is polydispersity in the branch length, however, can be very difficult even at low levels of polydispersity.

C. Regular H Chains. Predictions of the dynamic properties of regular H chains are illustrated in Figures 6–8. Their properties are not always distinct from those of linear chains or four-arm regular stars, but when they are, n_0/n_b is between 2 and 10 and the plateau region of the reduced angle characteristically has two levels; the lowest level is found at low frequency and never spans much more than a decade in frequency. The spectrum for regular H chains has a set of n_b doubly degenerate relaxation times, and a set of $n_0 + 1 + 2n_b$ nondegenerate relaxation times. The degenerate relaxation times are identical with those found in a regular star with n_b beads per branch, and the nondegenerate relaxation times are roughly the same as those found in a linear chain with $n_0 + 2 + 2n_b$ beads, when computed at the same h^*. Their spectral breadths can be quite different and are described by eq 19 and roughly by eq 18 (with $n_0 + 2 + 2n_b$ substituted for n_0), respectively. The longest relaxation time is always nondegenerate and is substantially larger than all others when $n_0/n_b \gg 1$. The shortest when $n_0 = 0$, or the two shortest when $n_0 > 0$, are also nondegenerate and distinctly separated from the rest of the spectrum. The presence of the two shortest modes, when $n_0 > 0$, is difficult to distinguish; they seldom differ by more than 4% and appear as a single, nondegenerate line.

The reduced properties of regular H chains depend on n_0, n_b, and h^*. The effects of n_0, the number of backbone beads between the two branch sites, are shown in Figure 6 for several chains with $n_b = 20$ and $h^* = 0.15$. Also shown are predicted properties of a four-arm regular star ($f = 4$, $n_b = 20$, $h^* = 0.15$) to demonstrate the starlike character of regular H chains when $n_0/n_b \ll 1$; its reduced magnitude and angle curves, represented by broken lines (short dashes), are virtually the same as that of the regular H chain with $n_0 = 0$. Similarly, the properties for a linear chain ($n_0 = 842$, $h^* = 0.15$) are also included to show the linear-chain character of regular H chains when $n_0/n_b \gg 1$; the magnitude and angle curves are again represented by broken lines (long dashes), and the curves superpose with those of the regular H chain with $n_0 = 800$. Unique characteristics of regular H chains are best found for $0.5 < n_0/n_b < 5$. As n_0/n_b increases from 0 to 1, the steepness of the low-frequency transition zone in the reduced angle drops, the level of the plateau region remains roughly the same, and the plateau breadth increases. As n_0/n_b approaches 2, the plateau region is displaced to higher reduced frequency and a second, lower level plateau appears at low frequency. The level and breadth of the high-frequency plateau do not change since they are primarily controlled by the degenerate relaxation times. The low-frequency plateau actually appears at a level below that of a long linear chain for the same h^*, and its breadth extends with increasing n_0/n_b but never exceeds much more than a decade of frequency. As n_0/n_b increases to

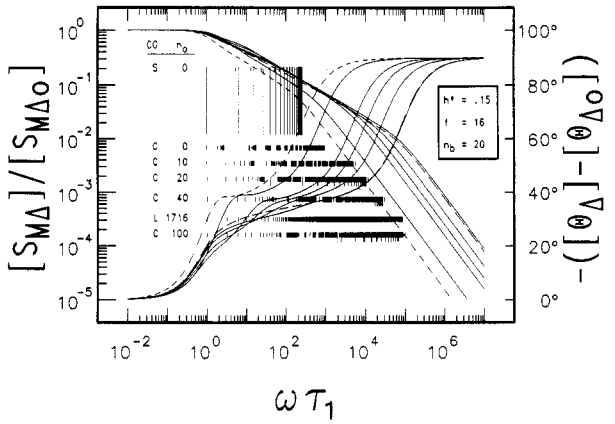

Figure 9. Effect of n_0 on predicted properties for regular combs. Curves corresponding to the top spectrum (a regular star) are drawn with short broken lines. Curves corresponding to the linear chain are drawn with long broken lines.

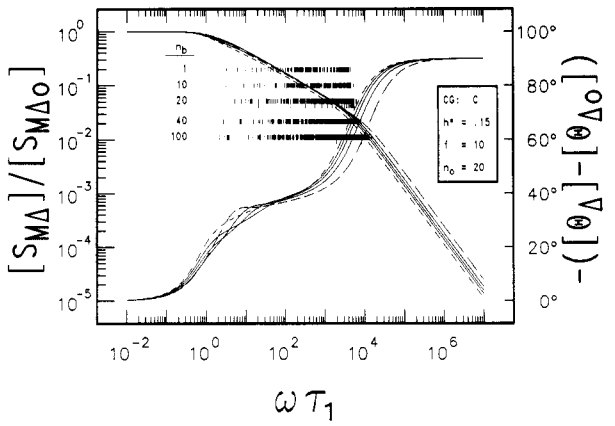

Figure 10. Effect of n_b on predicted properties for regular combs.

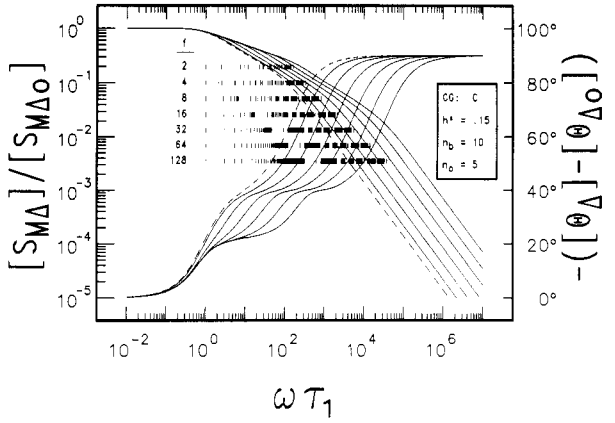

Figure 11. Effect of f on predicted properties for regular combs.

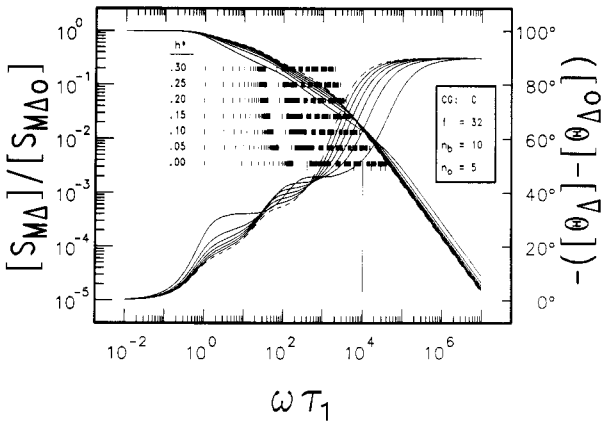

Figure 12. Effect of h^* on predicted properties for regular combs.

10, the levels of both plateaus approach those of linear chains. The same features are also visible in Figure 7 which illustrates the effects of varying n_b, the number of beads in each of the four branches, at $n_0 = 20$ and $h^* = 0.15$. However, more of the chains shown here are starlike than those in Figure 6. Note that the reduced angle of regular H structures always monotonically increases with increasing frequency.

The effects of h^* on the dynamic properties of regular H structures are shown in Figure 8. The chain chosen for this illustration has an n_0/n_b ratio of 5 to ensure the appearance of a two-level plateau in the reduced angle. As before, increasing h^* redistributes and decreases the spacings between the relaxation times. The breadths of both plateau regions shorten and their levels drop.

To fit data for monodisperse samples of regular H chains one would again use the h^* established for the polymer/solvent system from dynamic data for linear chains. The values of n_b and $n_0 + 1 + 2n_b$ would then be found by fitting the breadth of the high-frequency plateau and the breadth of the whole plateau region, respectively. Again, it should be verified that the fit parameters also describe the frequency dependence of the reduced magnitude. Samples with polydispersities in n_0, or in n_b, even at small levels, will degrade the fit. In addition, it will be difficult to unambiguously ascertain the chain geometry from dynamic data when n_0/n_b is extremely small or large; for these cases the data should be fit by using predictions for four-arm regular stars or linear chains, respectively.

D. Regular Combs. Predicted dynamic properties of regular combs are shown in Figures 9–12. Their properties can be similar to those of f-armed regular stars or linear chains, but more often they have their own unique characteristics. The most striking difference is the two-level plateau region in the reduced angle. These levels are most distinct when h^* is small and when the chain is highly branched ($f > 10$) and the branches are not extremely long or short ($0.2 < n_0/n_b < 5$). The reduced angle also has a strong dependence on f when such two-level plateaus are present. This dependence on f, in contrast to that predicted for regular stars, should enable the degree of long-chain branching in combs to be characterized at much higher levels.

The reduced properties of regular combs depend on f, n_0, n_b, and h^*. Their relaxation time spectrum is usually composed of nondegenerate times. Some doubly degenerate modes do occur and occasionally one mode in the free-draining limit can be $(f-1)$-fold degenerate (see Figure 12). The most degenerate modes are found when $n_0 = n_b$. In this case n_b of the modes are doubly degenerate; the degenerate modes only depend on n_b and h^* and are identical with the degenerate modes of regular star and H chains. Other degenerate modes are observed when n_0/n_b is an integer and f, n_0, and n_b share a common integer factor; these modes always have short relaxation times. The overall breadth of the relaxation time spectrum is controlled by the longest contiguous span within the chain. This span is composed of $(f-1)(n_0+1) + 2n_b$ or $f(n_0+1) + n_0 - 1$ springs, depending on whether n_0 is less or greater than n_b. Equation 18 provides good estimates of the breadth when N_{span} is substituted for n_0. The longer relaxation times are always nondegenerate; their spacings decrease as the chains become more starlike ($n_0 \ll n_b$). For starlike chains a group of $f-1$ relaxation times is distinctly separated from the others and as a group dominates the low-frequency properties. For all other combs the spacings of the first few modes are roughly that found in linear

chains composed of N_{span} springs and computed with the same h^*. The shortest relaxation times are separated from the others and are always nondegenerate. The number of such modes is either $f - 2$ or f depending on whether $n_0 = 0$ or $n_0 > 0$; their values are all quite similar and frequently this set of shortest modes appears as a single line in the drawn spectra. The separation of this group of modes from the others on the reduced frequency axis is similar to that found for three-arm stars when computed for the same h^*. These features are consistent with the observation that a short relaxation time, separated from the other modes, occurs for each branch site with a functionality of 3 or more and is smaller by a factor proportional to its functionality.

The effects of n_0, the number of backbone beads between adjacent branch sites (and the number of beads from the end of the backbone to the first branch site), on the frequency dependence of $[S^*]_\Delta/[S_0]_\Delta$ are shown in Figure 9 for combs with $f = 16$, $n_b = 20$, and $h^* = 0.15$. Included in this figure are the properties of a regular star ($f = 16$, $n_b = 20$, $h^* = 0.15$) and a linear chain ($n_0 = 1716$, $h^* = 0.15$) to show that the reduced properties of some regular combs may be difficult to distinguish from those of simpler chain geometries. The frequency dependence of $[S^*]_\Delta/[S_0]_\Delta$ for the regular star (broken line) is essentially that of the comb with $n_0 = 0$; only a small shift in the reduced frequency is required to make them superpose. Starlike character in combs always arises when $n_0/n_b \ll 1$. Likewise the frequency dependence of $[S^*]_\Delta/[S_0]_\Delta$ for the linear chain (broken line) closely approximates that of the comb with $n_0 = 100$. The reduced properties become indistinguishable from those of linear chains when $n_0/n_b \gg 1$. The characteristic two-level plateau region in the reduced angle is best observed in Figure 9 for combs with $n_0 = 10$, 20, or 40. For the same f and h^*, the higher level, high-frequency plateau shifts to higher reduced frequency as n_0/n_b increases; its breadth, controlled by the intrachain length of $2n_b + n_0 + 1$ springs, also increases, while its level remains constant. Concomitantly, as n_0/n_b increases, the lower level, low-frequency plateau increases in breadth and rises in its level. The breadth is roughly controlled by the intrachain length of $f(n_0 + 1)$ springs when $fn_0 \gg n_b$. Many of these same features are also visible in Figure 10, which illustrates the dependence of the dynamic properties on n_b, the number of beads per branch, for regular combs ($f = 10$, $n_0 = 20$, $h^* = 0.15$). This plot best illustrates the dramatic changes occurring in the low-frequency transition zone of reduced angle as starlike behavior is approached.

The effects of f, the number of branches attached to the backbone, are illustrated in Figure 11. Here chains have a n_0/n_b ratio of 0.5 so that the characteristic two-level plateau of combs can be seen. As f increases from 2 to 128, the level of each plateau region and the breadth of the high-frequency plateau remain approximately invariant. Only the breadth of the low-frequency plateau increases; it is primarily controlled by the intrachain length $f(n_0 + 1)$ and hence has a strong dependence on f. This dependence on f is much stronger than that predicted for regular stars and suggests an excellent potential for use of solution dynamics for characterizing the degree of branching in highly branched regular combs.

The degree of hydrodynamic interaction affects the properties of regular combs in much the same manner as for other geometries as is illustrated in Figure 12 ($n_0 = 5$, $n_b = 10$, $f = 32$). As h^* increases, relaxation time spacings rearrange and the overall spectral breadth decreases. As a result the level of each plateau drops and their breadths narrow.

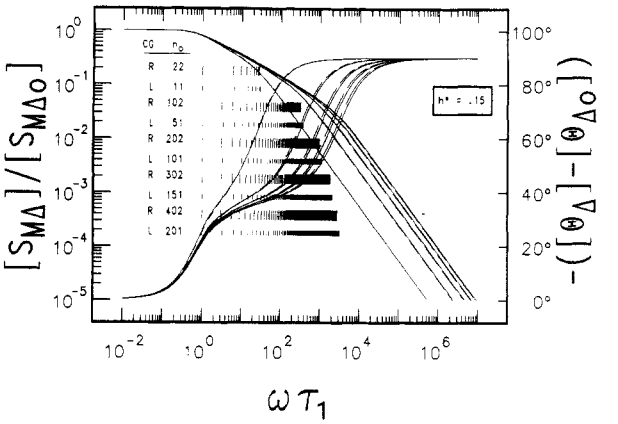

Figure 13. Comparison of properties for linear chains and rings when $h^* = 0.15$. Reduced properties of linear chains (solid lines) roughly superpose with those of rings (broken lines) when the rings contain twice the number of beads; superposition is best at small n_0.

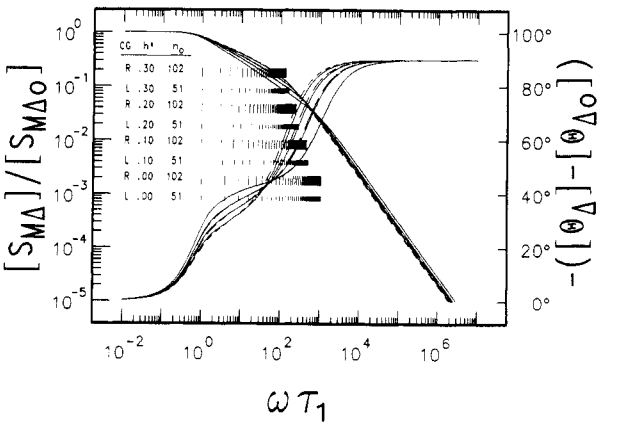

Figure 14. Comparison of properties for linear chains (solid lines) and rings (broken lines). The reduced properties for a linear chain ($n_0 = 51$) fit the properties for a ring ($n_0 = 102$) best when h^* is small.

Model parameters f, n_0, and n_b are assigned to fit measured properties of regular combs after h^* has been established for the polymer/solvent system on the basis of results for linear chains. The data are first inspected for characteristics of linear chains or regular stars. If either is present, the properties are fit to these simpler structures as outlined in previous sections. Otherwise, the breadth of the high-frequency plateau establishes the intrachain length of $2n_b + n_0 + 1$ springs, while the level and breadth of the low-frequency plateau establish the n_0/n_b ratio and f, respectively. Sample polydispersity in f, n_0, or n_b will make the assignment of each parameter more difficult. The effects of randomly attaching f branches along the straight-chain backbone is also not well understood. However, it is known[4,20] that the predictions for regular combs are at least semiquantitatively correct for the OFB properties of randomly branched combs.

E. Rings. Figures 13 and 14 show predictions of the solution properties for rings and linear chains. The relaxation time spectra of rings[25,35] is composed of $(n_0 - 1)/2$ or $(n_0 - 2)/2$ doubly degenerate modes depending on whether n_0 is odd or even, respectively. All the modes are degenerate when n_0 is odd, but one mode is nondegenerate when n_0 is even. The longest mode is always degenerate and is substantially larger than the others when $n_0 > 200$. The smallest is degenerate (n_0 odd) or nondegenerate (n_0 even). The reduced properties are functions of n_0 and h^*. The number of beads in the chain n_0 is proportional to the

contour length of the chain. The effects of n_0 on the frequency dependence of $[S^*]_\Delta/[S_0]_\Delta$ are shown in Figure 13 for $h^* = 0.15$. As for linear chains, increasing n_0 increases the number of the relaxation times and the breadth of the spectrum and thus enlarges the breadth of the single-level plateau region of the reduced angle. The effects of h^* are shown in Figure 14. Increasing h^* redistributes the spacings of the relaxation times and compresses the spectral breadth, which lowers the level and reduces the breadth of the plateau region of the reduced angle. The level of the low-frequency portion of the plateau region depends only on h^* for large chains ($n_0 > 200$); it drops about 10° at $\omega\tau_1 = 10$ as h^* increases from 0 to 0.30.

The spacings of the longer relaxation times depend primarily on h^* when $n_0 > 200$. Such spacings for chains of finite size agree well with those reported at the two draining limits by Bloomfield and Zimm[25] for infinitely long rings. They found the τ_1/τ_p ratios for the first six modes to be

$$1, 4, 9, 16, 25, 36, \ldots \quad \text{for} \quad h^* = 0.00$$

and

$$1, 2.90, 5.36, 8.29, 11.16, 15.27, \ldots \quad \text{for} \quad h^* = 0.25$$

As for linear chains, τ_1 exceeds the other τ_p by a factor of about 3 or more.

The breadth of the relaxation time spectrum may be estimated at the two draining limits for long chains. Expressions for λ_1 at both limits and λ_N for the free-draining limit are given by Bloomfield and Zimm. The value of λ_N, 2.29, at the non-free-draining limit ($h^* = 0.25$) is taken from our computations for chains of finite size and $n_0 > 200$. Combining these results yields

$$\begin{aligned} \tau_1/\tau_N &\simeq (1/\pi)^2 n_0^2 \quad \text{for} \quad h^* = 0.00; \quad n_0 > 100 \\ &\simeq 0.172 n_0^{1.5} \quad \text{for} \quad h^* = 0.25; \quad n_0 > 100 \end{aligned} \tag{20}$$

The exponent diminishes from 2 to 1.5 and the prefactor rises from 0.101 to 0.172, as h^* increases from 0.00 to 0.25; both limiting power-law relationships indicate that the breadth has a much stronger dependence on n_0 than on h^*. Comparison of these spectral breadths to those of linear chains, eq 18, indicates that those of linear chains are larger by a factor of 3.3–4.0.

Assigning model parameters to fit the dynamic properties of monodisperse samples of rings follows the same procedure used for linear chains. The method works best when dynamic data are available for a set of ring samples with the same repeat unit but with differing molecular weights. h^* is ascertained from the level of the low-frequency portion of the plateau region of the high molecular weight samples; n_0 is then adjusted until the breadth of the plateau region is fit. Small amounts of polydispersity are expected to effect only the assignment of n_0.

The frequency dependences of $[S^*]_\Delta/[S_0]_\Delta$ for ring and linear chains are very similar when the ring is composed of twice as many beads. This can also be seen in Figures 13 and 14. The properties are most similar when h^* and chain length are small; then the properties for rings (broken lines) superpose on those for linear chains (solid lines). The strong similarity of such properties poses a problem in the identification of chain geometry for an unknown sample. For this case, the properties of the unkown should be compared to those of a set of monodisperse samples of linear standards used to assign the value of h^*. First, an n_0 is found to fit the dynamic data by using BSM predictions for linear chains. Second, the

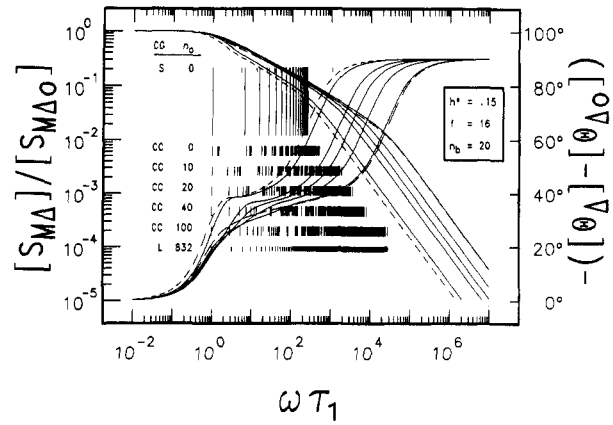

Figure 15. Effect of n_0 on predicted properties for regular cyclic combs. Curves corresponding to the top spectrum (a regular star) are drawn with short broken lines. Curves corresponding to the linear chain are drawn with long broken lines.

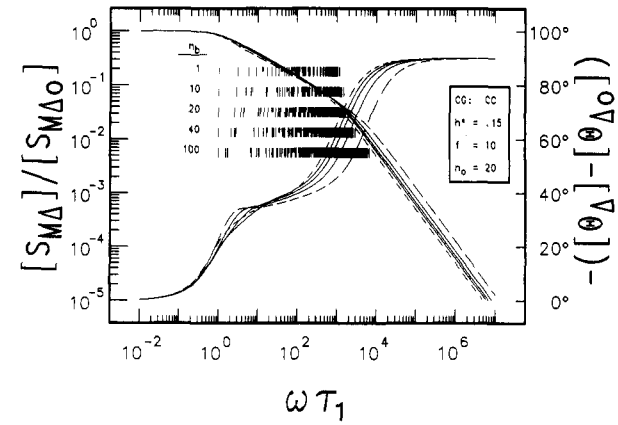

Figure 16. Effect of n_b on predicted properties for regular cyclic combs. Curves corresponding to the top spectrum ($n_b = 1$) are drawn with short broken lines. Curves corresponding to the bottom spectrum ($n_b = 100$) are drawn with long broken lines.

relationship between the n_0 and molecular weight of the unknown (obtained from an auxiliary experiment such as light scattering) is compared to that for linear standards. The chain geometry of the unknown sample is linear when M/n_0 is consistent with the standards; it has ring geometry when M/n_0 is twice that expected for linear chains. The relationship between $[S_0]_\Delta$ and n_0 could also be used to determine chain geometry with a similar procedure; this method would avoid determining the molecular weight of the unknown sample by a separate experiment. For this case $[S_0]_\Delta$ for linear chains would be 1.5–2.0 times larger than that for rings at the same n_0. The factor depends on h^* and only weakly on n_0 when $n_0 > 100$. The factor monotonically rises as h^* decreases; the two extremes represent the two draining limits.

The strong similarity of the properties of linear and ring chains is advantageous for fitting the properties of long linear chains since laborious numerical computations of the λ_p can be avoided. The properties can be fit with predictions for rings based on λ_p computed with a recently reported simple closed-form expression.[35] The true n_0 for the linear chain is then well approximated by dividing the n_0 obtained from this fit by two.

F. Regular Cyclic Combs. Solution properties of regular cyclic combs are predicted in Figures 15–18. These chains have f arms (n_b beads per arm) attached at equal intervals around a cyclic backbone of $f(n_0 + 1)$ beads. The frequency dependence of $[S^*]_\Delta/[S_0]_\Delta$ for cyclic combs is very similar to that for regular combs when computed for the same f, n_b, and h^*, but with twice the n_0. Hence such

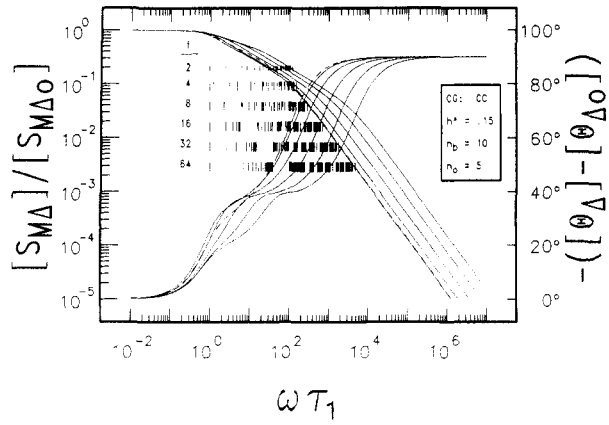

Figure 17. Effect of f on predicted properties for regular cyclic combs.

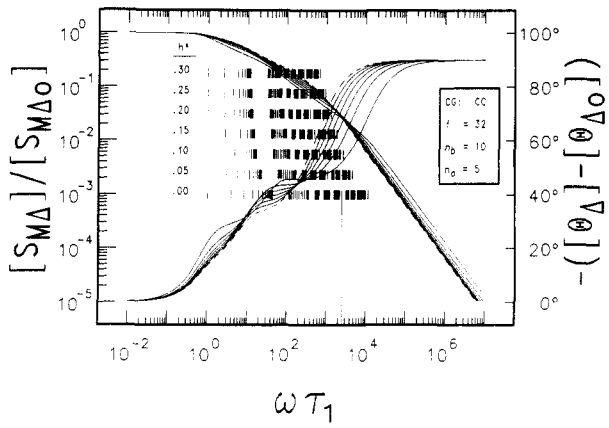

Figure 18. Effect of h^* on predicted properties for regular cyclic combs.

properties appear like those for f-armed regular stars when $n_0/n_b \ll 1$ and like linear chains when $n_0/n_b \gg 1$, or they have a characteristic two-level plateau in the reduced angle when the chain has many branches ($f > 10$) and the branches are not extremely long or short ($0.4 < n_0/n_b < 10$). The properties of cyclic combs also have a strong dependence on f, which again predicts that the degree of branching can be characterized for highly branched chains.

The assignment of model parameters, f, n_0, and n_b, when fitting dynamic properties for monodisperse samples of regular cyclic combs, parallels that for combs. The only differences are that the breadth of the high-frequency plateau region is used to establish the intrachain length of $(n_0 + 1)(1 - f^{-1}) + 2n_b$ equivalent springs, and the breadth of the entire (two-level) plateau is used to roughly establish the intrachain length $[(n_0 + 1)(f - 1)/2 + 2n_b$ or $(n_0 + 1)f/2 + 2n_b$ when f is odd or even, respectively].

G. Identification of Chain Geometry. The chain geometry of an unknown homopolymer sample is predicted to be identifiable in the following way if it has one of the six simple geometries. First, the absence of sample polydispersity should be verified by determination of the absolute number- and weight-average molecular weights ($\bar{M}_n$ and $\bar{M}_w$) from osmometry and light-scattering experiments; a relative characterization of both molecular weight averages by size exclusion chromatography experiments would also be sufficient. Second, the dynamic properties should be measured over a range of shearing frequencies sufficient to fingerprint the low-frequency transition zone and the complete plateau region and then extrapolated to infinite dilution as outlined in section II.B. The chain geometry would be identified as linear, ring, or regular star if the plateau region of the measured properties has a single level; it would be identified as a regular star, a starlike regular comb, or a starlike regular cyclic comb if the low-frequency portion of the plateau region has a local minimum and maximum; it would be identified as a regular H, regular comb, or regular cyclic-comb chain if the plateau region has two levels. (If no plateau is observed and the reduced angle changes from 0 to 90° in less than three decades of shearing frequency, the chain is probably too small to determine its geometry.) Any further differentiation between chain geometries requires the availability and analysis of several samples of linear chains that have the same repeat unit as the unknown and that cover a reasonably wide range of molecular weights. The dynamic properties of these linear samples would be measured in the same solvent as the unknown and then used to ascertain the degree of hydrodynamic interaction appropriate for this polymer/solvent system. Regular stars would then be differentiated from linear chains and rings at this h^* by the higher levels of their plateau regions in the reduced angle; rings would be differentiated from linear chains with $[S_0]_\Delta$ and n_0 as detailed in section IV.E. Differentiation among starlike chains with local extrema in the reduced angle would be the most difficult; it is probable that these chains can only be simply characterized as regular stars. Regular comb and cyclic-comb chains would be differentiated from regular H chains from estimates of the degree of branching. If the value of f required to fit the data with regular-comb predictions exceeds 2, the unknown is a comb or cyclic comb structure; otherwise the data should be fit to the predictions for regular H chains because they are simpler than the others. Differentiation between regular combs and cyclic combs would require knowledge of $[S_0]_\Delta$ and n_0. The method parallels that used to discern linear from ring chains. All of the above procedures presume that enough is known about the synthesis of the sample to assure it has one and only one of the six simple geometries. Otherwise, even though the solution properties might be well fit by predictions for one chain geometry, that geometry would not be confirmed absolutely. At best, the data could be reported as being consistent with this geometry.

V. Conclusions

Measurements of the frequency dependence of $[S^*]_\Delta$ or $[\eta^*]_\Delta$ are predicted to be very useful in characterizing the long-chain structure of monodisperse samples of flexible homopolymers. These solution properties enable the identification of chains with linear, regular star, regular H, regular comb, ring, or regular cyclic-comb geometries subject to the restrictions summarized in section IV.G. Some identifications will require additional measurements of a few molecular weight standards with linear geometry and the same repeat unit to aid the interpretation. Furthermore, after one of these chain geometries is established, the number of branches attached to the backbone, the spacing between branch sites on the backbone, and the sizes of the branches and backbone can also be characterized, in general. The only predicted limitation is the evaluation (from the "high-frequency" subplateau) of the number of branches at a branch site when its functionality exceeds 8. This limitation is seen in regular stars and starlike combs or cyclic combs where the f arms are essentially attached at the same site. (A subsequent publication[41] with BSM predictions of regular brushes—regular combs but with each branch site having a functionality of 3 or more—will demonstrate that the level of the "low-frequency" plateau should be useful for characterizing the functionality of branch sites at higher levels (<50).) The degree of hydrodynamic interaction has only a small effect

on the characterization of such long-chain structure. Increasing h^* always shortens the breadth and lowers the level of the plateau region of the reduced angle. This result indicates that characterization is best when h^* is small and hence favors the measurement of dynamic properties in good solvents.

In addition, the low-shear-rate dynamic properties of starlike combs or cyclic combs are predicted to be so similar to those of regular stars that these structures, which are less sterically hindered and thus easier to synthesize, could be substituted for regular stars. Likewise, the properties for combs or cyclic combs with $n_0/n_b \gg 1$ and those for rings appear very much like those for linear chains, but here there is no synthetic advantage because the linear chains are simpler to make. On the other hand, for those fitting dynamic data, the similarity between the properties of linear chains and rings with twice the contour length is advantageous. The properties of rings can be computed much more efficiently with the recently published closed-form eigenvalue expressions valid for all h^*. All predictions reported here, or carried out to date, are consistent with the relaxation time spectrum breadth depending on the length of the longest contiguous span within the chain; hence for chains composed of the same number of springs, the widest spectral breadths are associated with chains having the fewest branches and/or rings.

Acknowledgment. We express our appreciation to Emeritus Professor J. D. Ferry for helpful discussions. This work was supported by the National Science Foundation Polymers Program through Grants DMR-7925020 and DMR-8303207.

References and Notes

(1) Birnboim, M. H.; Ferry, J. D. *J. Appl. Phys.* **1961**, *32*, 2305.
(2) Johnson, R. M.; Schrag, J. L.; Ferry, J. D. *Polymer* **1970**, *1*, 742.
(3) Soli, A. L.; Schrag, J. L. *Macromolecules* **1979**, *12*, 1159.
(4) Dibbs, M. G. Ph.D. Thesis, University of Wisconsin at Madison, 1983.
(5) Sammler, R. L. Ph.D. Thesis, University of Wisconsin at Madison, 1985.
(6) Stokich, T. M. Ph.D. Thesis, University of Wisconsin at Madison, 1988.
(7) Thurston, G. B.; Schrag, J. L. *Trans. Soc. Rheol.* **1962**, *6*, 325.
(8) Miller, J. W. Ph.D. Thesis, University of Wisconsin at Madison, 1979.
(9) Lodge, A. S.; Wu, Y. *Rheol. Acta* **1971**, *10*, 539. Rheology Research Center Report No. 16; University of Wisconsin: Madison, 1972.
(10) Sammler, R. L.; Schrag, J. L. *Macromolecules* **1988**, *21*, 1132.
(11) Sakanishi, A. *J. Chem. Phys.* **1968**, *48*, 3850.
(12) Osaki, K.; Mitsuda, Y.; Johnson, R. M.; Schrag, J. L.; Ferry, J. D. *Macromolecules* **1972**, *5*, 17.
(13) Osaki, K.; Schrag, J. L.; Ferry, J. D. *Macromolecules* **1972**, *5*, 144.
(14) Warren, T. C.; Schrag, J. L.; Ferry, J. D. *Macromolecules* **1972**, *6*, 467.
(15) Mitsuda, Y.; Schrag, J. L.; Ferry, J. D. *Polym. J. (Tokyo)* **1973**, *4*, 24.
(16) Mitsuda, Y.; Schrag, J. L.; Ferry, J. D. *Polym. J. (Tokyo)* **1973**, *4*, 668.
(17) Lodge, T. P.; Miller, J. W.; Schrag, J. L. *J. Polym. Sci., Polym. Phys. Ed.* **1982**, *20*, 1409.
(18) Lodge, T. P.; Schrag, J. L. *Macromolecules* **1982**, *15*, 1376.
(19) Martel, C. J. T.; Lodge, T. P.; Dibbs, M. G.; Stokich, T. M.; Sammler, R. L.; Carriere, C. J.; Schrag, J. L. *Faraday Symp. Chem. Soc.* **1983**, *No. 18*, 173.
(20) Peterson, P. S.; Dibbs, M. G.; Sammler, R. L.; Fetters, L. J.; Roovers, J. E. L.; Schrag, J. L., in preparation.
(21) Kirkwood, J. G.; Riseman, J. *J. Chem. Phys.* **1948**, *16*, 565.
(22) Rouse, P. E. *J. Chem. Phys.* **1953**, *21*, 1272.
(23) Zimm, B. H. *J. Chem. Phys.* **1956**, *24*, 269.
(24) Zimm, B. H.; Kilb, R. W. *J. Polym. Sci.* **1959**, *37*, 19.
(25) Bloomfield, V.; Zimm, B. H. *J. Chem. Phys.* **1966**, *44*, 315.
(26) Osaki, K.; Schrag, J. L. *J. Polym. Sci., Polym. Phys. Ed.* **1973**, *11*, 549.
(27) Osaki, K.; Mitsuda, Y.; Schrag, J. L.; Ferry, J. D. *Trans. Soc. Rheol.* **1974**, *18*, 395.
(28) Bird, R. B.; Hassager, O.; Armstrong, R. C.; Curtiss, C. F. *Dynamics of Polymeric Liquids: Kinetic Theory*; Wiley: New York, 1977; Vol. II, Chapter 12.
(29) Schrag, J. L. *Trans. Soc. Rheol.* **1977**, *21*, 399.
(30) Landry, C. J. T. Ph.D. Thesis, University of Wisconsin at Madison, 1985.
(31) Merchak, P. M. Ph.D. Thesis, University of Wisconsin at Madison, 1987.
(32) Thurston, G. B.; Peterlin, A. *J. Chem. Phys.* **1967**, *46*, 4881.
(33) Osaki, K. *Macromolecules* **1972**, *5*, 141.
(34) Wilkinson, J. H. *The Algebraic Eigenvalue Problem*; Oxford University Press: 1965.
(35) Liu, T. W.; Öttinger, H. C. *J. Chem. Phys.* **1987**, *87*, 3131. Rheology Research Center Report No. 110; University of Wisconsin: Madison, 1987.
(36) Thurston, G. B.; Morrison, J. D. *Polymer* **1969**, *10*, 421.
(37) Thurston, G. B. *Polymer* **1974**, *15*, 569.
(38) Perico, A.; Piaggio, P.; Cuniberti, C. *J. Chem. Phys.* **1975**, *62*, 4911.
(39) Thurston, G. B.; Schrag, J. L. *J. Chem. Phys.* **1966**, *45*, 3373.
(40) Thurston, G. B. *J. Chem. Phys.* **1967**, *47*, 3582.
(41) Sammler, R. L., in preparation.
(42) Hadjichristidis, N.; Roovers, J. E. L. *J. Polym. Sci., Polym. Phys. Ed.* **1974**, *12*, 2521.
(43) Roovers, J. E. L.; Bywater, S. *Macromolecules* **1972**, *5*, 384.
(44) Roovers, J. E. L.; Hadjichristidis, N.; Fetters, L. J. *Macromolecules* **1983**, *16*, 214.